Industrial Crops & Products 211 (2024) 118225

Contents lists available at ScienceDirect

Industrial Crops & Products

journal homepage: www.elsevier.com/locate/indcrop

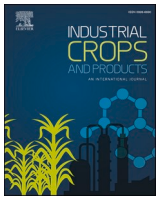

Effect of alkaline catalysts on the valorization of sugarcane bagasse via pyrolysis

Morayma Muñoz [a], Marco Rosero [a], Angela N. García [b,*], Antonio Marcilla [b]

[a] Chemical Engineering Faculty, Central University of Ecuador, Calle Ritter s/n & Bolivia, Quito 170129, Ecuador
[b] Department of Chemical Engineering, University of Alicante, P.O. Box 99, Alicante E-03080, Spain

ARTICLE INFO

Keywords:
Pyrolysis
Sugarcane bagasse
Alkaline treatment
Alkaline catalyst
TGA
FTIR
GC/MS

ABSTRACT

Sugarcane bagasse (Saccharum officinarum) is a widely spread residual biomass from the sugar industry that can be valorized through pyrolysis. The spectrum of the fractions obtained will vary depending on the pyrolysis conditions selected. In this work, the influence of alkaline treatments on the raw material has been studied. The sugarcane residues were treated with sodium or potassium hydroxides (1:1 sample/hydroxide ratio) and subsequently washed to remove hydroxides. Slow pyrolysis in a thermobalance connected to FTIR and flash pyrolysis in an EGA/Py-GC/MS system were performed with three types of samples, i.e.: raw material, hydroxides impregnated bagasse and the material obtained after washing the previous impregnated samples to remove the hydroxides. The experiments carried out allow us to distinguish between the effect of the basic pretreatment and the catalytic effect of the alkaline ions present during the pyrolysis on the compounds generated, thus allowing us to analyze the advantages that these processes can present in the bagasse valorization. According to the results obtained, the presence of alkaline ions in the sample during the pyrolysis process increases char percentage very significantly as well as cyclopentanone and cyclopentenone derivatives and the amount of CO_2 evolved, reducing levoglucosane drastically and the vinyl and methoxy groups in the volatiles obtained. The washing treatment until neutral pH, after the alkaline impregnation, modifies the spectrum of pyrolytic products obtained, reducing phenol derivatives and increasing very significantly the percentage of levoglucosane and hydroxiacetaldehyde. Thus, the changes in the bagasse structure as well as in the decomposition mechanism could be tuned to produce activated carbon in a single step (maximizing carbon yield), diminishing the oxygen content in the bio-oil obtained (increasing its heating value) and reducing the pyrolytic compound spectrum (increasing the selectivity of the process).

1. Introduction

The annual production of lignocellulosic biomass is about 181.5 billion tons originated from forests and crops (43%), grasslands (42%) and agricultural waste (15%) (Deng et al., 2023). These materials can be a useful feedstock to produce sustainable fuels and added-value products. In this context, a wide review about the conversion of lignocellulosic biomass into fuels and chemicals has been published recently (Deng et al., 2023). Pyrolysis appears as an efficient way for treating this type of residues, obtaining products with high potential, fuels for energy use and chemicals for different industrial sectors.

The pyrolysis process is the addition of multiple complex primary and secondary reactions that transform the biomass into three pyrolytic fractions (bio-oil, biogas and biochar). The percentage and composition of these fractions depends on the characteristics of the raw material (type of biomass, elemental composition, ash content, particle size…) but also on the operating parameters, such as temperature, heating rate, residence time, sample pretreatments or catalyst used. Amenaghawon et al. (2021) analyzed the state-of-the-art of biomass pyrolysis technologies for the obtention of added-value products.

The role of the catalyst in pyrolysis can be to reduce the decomposition temperature but, even more important, to increase the selectivity of the process, prioritizing some reactions over others, reducing the number of compounds generated and increasing their yield. The catalytic effects of alkaline metals on the pyrolysis process have been widely studied; in fact, the ash content of the raw material acts as catalyst in the process. An extensive review about these aspects has been recently published (Wang et al., 2022a). Besides as catalysts, alkaline metals are

* Corresponding author.
E-mail address: angela.garcia@ua.es (A.N. García).

https://doi.org/10.1016/j.indcrop.2024.118225
Received 14 December 2023; Received in revised form 1 February 2024; Accepted 7 February 2024

also used in chemical pretreatments of lignocellulosic biomass. This type of pretreatments allows isolating the components of the raw material. An alkaline hydrolysis can solubilize the lignin fraction of the biomass and remove the acetyl units of the hemicellulose, facilitating the enzymatic hydrolysis of cellulose. Recent advances in physical and chemical pretreatments are compiled by Mankar et al. (2021). Therefore, an alkaline pretreatment can modify the sample structure while the presence of alkaline metals during the pyrolysis process can alter the decomposition mechanisms.

The generally accepted tendency is that the presence of alkali and alkaline earth metals in biomass shifts its decomposition temperature towards lower values, increases the yield of char and gases and decreases the production of bio-oil. However, apparently contradictory behaviors can be found in the literature, due to the high number of factors that influence the process (Wang et al., 2022a). Thus, DeGroot and Shafizadeh (1984) observed that the pyrolysis of wood after incorporating potassium through ion exchange followed the general tendency, while by adding calcium, the effect observed was the opposite: increase of decomposition temperature and only slight influence on char yield. Moreover, they also noticed differences in the results depending on the method of adding the same cation to the biomass. Thus, when potassium was incorporated into cellulose by absorption of potassium carbonate in solution, its decomposition temperature increased significantly. Zhou et al. (2013) indicated the different effects of the K^+ ion depending on the concentration in which it is found: at high concentrations, K^+ promotes fragmentation reaction while at lower concentrations, it favors depolymerization mechanism. The influence of the anion accompanying the cation seems to influence the results obtained, but it also depends on the operating conditions. For example, KOH and KCl decrease the yield of levoglucosan in cellulose pyrolysis. Both catalysts have a similar effect, but while Marathe et al. (2017) obtained that KOH reduces the levoglucosan yield more than KCl, Fu et al. (2019) concluded the opposite.

Hydroxides and salts of sodium and potassium are used as chemical activators in the processes to obtain active carbon. Traditionally, the activation process is carried out in two steps: hydrothermal carbonization or pyrolysis followed by the activation process of the char obtained previously. Any attempt to carbonize and activate in a single step seems to produce chars with worse properties. However, Balahmar et al. (2017) reported results of carbonization and activation in a single step, from different types of biomass using KOH as activating agent. The properties of the activated carbons obtained were similar or better than those reached in a two-stage process. Shen et al. (2020) used the catalytic pyrolysis of rice hulls with hydroxide and different salts of potassium for the co-production of biofuels and porous carbons.

According to these results, the optimization of the activation process in a single step, with the appropriate catalyst, could increase the yield of activated carbon by benefiting from the increase in the yield of char during catalytic pyrolysis, reducing costs without decreasing the quality of the product.

The sugarcane is a lignocellulosic biomass used worldwide as a raw material to produce sugar. The total production of sugarcane reached nearly $1.9{\cdot}10^9$ tons in 2021 with Brazil, India and China as the main producers (The Science Agriculture, 2023). In Ecuador, the production of sugarcane has maintained a growing trend in recent years to satisfy national demand. In addition to sugar production, sugarcane is also used to produce distilled alcoholic beverages obtained from the fermentation of sugary juice (CINCAE, 2013).

Sugarcane bagasse is the lignocellulosic fibrous residue obtained from the sugar agro-industry, where the cane juice is extracted. This represents approximately 30% by weight of the wet sugarcane plant (Wang et al., 2022b). Its annual worldwide production is about 540 million tons (Deng et al., 2023).

The chemical composition of sugarcane bagasse depends greatly on its origin. Different authors (Mahmud and Anannya, 2021; Antunes et al., 2022) present range of values for the hemicellulose, cellulose and lignin content according to data found in different references. Thus, percentages between 26% and 47% for cellulose, 19–33% hemicellulose, 14–23% lignin have been reported. Haghdan et al. (2016) presented increased percentage of lignin (25–32%) and included 6–12% of extractives. Almost 13% of extractives in bagasse is also considered by Kanwal et al. (2019). Wang et al. (2022b) emphasize the presence of soluble sugars in sugarcane bagasse, whose percentage is not often considered.

Due to the extent of this waste, there are various references where its valorization has been studied from different points of view, such as study of the extraction of sugar from sugarcane bagasse and use of the waste as an adsorbent (Wang et al., 2022b); review on the use of bagasse as biosorbent for removal of dyes (Aruna et al., 2021); methane obtention from anaerobic digestion (Costa et al., 2014) or extracted materials for composite material production (Mahmud and Anannya, 2021).

Several authors also reported studies about thermal decomposition of sugarcane bagasse, under different conditions. For example, Tsai et al. (2006) studied the fast pyrolysis of bagasse, among other residues, in an induction-heating reactor, analyzing the effect of pyrolysis temperature, heating rate and holding time on the yields of the products obtained. Schmitt et al. (2020) performed the fast pyrolysis of sugarcane bagasse at 500 °C in a twin-screw reactor, analyzing the gas and liquid fractions obtained. Kanwal et al. (2019) studied the torrefaction process of this residue at different temperatures and residence times. Catalytic pyrolysis of lignin extracted from sugarcane bagasse was studied, analyzing the phenol fraction obtained in the process (Naron et al., 2019) as well as the fast pyrolysis of bagasse hemicellulose at different temperatures in a tubular furnace, analyzing the fractions obtained (Peng and Wu, 2011). Antal et al. (1990) reviewed the yield of charcoal generated from the pyrolysis of sugarcane bagasse under different operating conditions. Kinetics of bagasse thermal degradation has also been performed, mainly from thermogravimetric analysis curves (Motaung and Anandjiwala, 2015; Mothé and de Miranda, 2013; Munir et al., 2009; Ounas et al., 2011)

In this paper, a systematic study on the thermal decomposition of sugarcane bagasse (untreated and alkali-treated samples) has been done, using different techniques and treatments and comparing the results obtained. No previous papers on analytical pyrolysis of this residue (neither untreated nor alkali-treated samples) focused on the pyrolysis process and the compounds obtained have been found.

The objective of this work is to study options to valorize sugarcane bagasse through pyrolysis, using Na and K hydroxides, both as catalysts for the carbonization process and for chemical pretreatment of the waste, analyzing the products obtained under different operating conditions.

The improved knowledge of possible processes for lignocellulosic waste valorization will contribute to the development of adequate technology for this purpose, thus allowing the improvement of more sustainable biorefineries.

2. Experimental section

2.1. Materials

The sugarcane bagasse (Saccharum officinarum) was a residual from agro-industrial processes derived from guarapo extraction processes for alcoholic fermentation, in Nanegal Canton, north-western province of Pichincha-Ecuador. The material was dried when received. Its original moisture content was 8.4%.

2.2. Treatments

As a previous stage, the sugarcane bagasse was triturated in a mill and passed through a No. 35 mesh sieve, to produce a sub-sample at diameter up to 0.5 mm.

Treatment 1: Alkali impregnation

The sugarcane bagasse sample was impregnated with a 1:1 ratio mixture with potassium hydroxide (KOH) (≥85% basis CAS number: 1310–58–3) or sodium hydroxide (NaOH) (pure ≥98% basis CAS number: 1310–73–2).

Approximately 5 g of sugarcane bagasse was treated with 5 g of KOH or NaOH dissolved in 50 mL of water at room temperature. The mixture was stirred for 30 min and oven-dried at 100 °C until constant weighing. During the drying process, the sample was manually mixed several times to ensure its homogeneity.

These catalysts have been selected for different reasons: they increase carbon yield and are also chemical activating agents, so they can be useful in obtaining active carbon in carbonization+activation processes. In addition, they are cheap and non-toxic compounds.

Treatment 2: Alkali removal

To remove alkaline hydroxides from samples, both treated with KOH and NaOH were washed with excess water 3–4 times, at room temperature, down to pH 7 (value checked by pH paper) and then oven dried at 100 °C until constant weight.

Sample identification

Sample S0: refers to the sugarcane bagasse.

Sample SK: bagasse sample impregnated with KOH solution.

Sample SNa: bagasse sample impregnated with NaOH solution.

Sample SKW: sample SK to which treatment 2 (washing) has been applied.

Sample SNaW: sample SNa to which treatment 2 (washing) has been applied.

2.3. Analysis methods

2.3.1. Proximate and ultimate analysis

The moisture of the original sample was determined by drying it in an oven at 110 °C until constant weight, according to the standard method ASTM-D3173–11.

Ash content was determined by sample calcination at 850 °C and gravimetric determination of the residue, according to ASTM D3174–12.

The equilibrium moisture content, volatiles and fixed carbon were determined from thermogravimetric analysis. Previous works (Karatepe and Küçükbayrak, 1993; García et al., 2013) demonstrated the similarity between the results of proximal analysis obtained by ASTM methods and TGA experiments, the second option being faster and simpler.

The elemental analysis of the sugarcane bagasse (C, N, H, S) was performed using an Elemental Microanalyzer Thermo Finnigan Flash 1112. Oxygen content in the sample was calculated by difference.

Potassium and sodium contents were analyzed by ICP-OES Perkin Elmer Optima 7300 DV.

2.3.2. High heating value (HHV) determination

The high heating value was calculated from Channiwala's correlation

$$HHV_{dry\ basis}\ (kJ\ kg^{-1}) = 349.1{\cdot}\%C + 1178.3{\cdot}\%H - 103.4{\cdot}\%O - 15.1{\cdot}\%N + 100.5{\cdot}\%S - 21.1{\cdot}\%A \quad (1)$$

which uses the elemental composition of the biomass for carbon (C), hydrogen (H), oxygen (O), nitrogen (N) and sulfur (S) as well as ash content (A) in mass percentage of dry material.

Channiwala and Parikh (2002) proposed this correlation to estimate the HHV of fuels. They analyzed 22 different correlations deduced by previous researchers and proposed one derived using 225 data and validated for additional 50.

Díaz (2008) estimated the HHV value of 3 different samples of sugarcane bagasse using 5 different correlations. The maximum error between the values obtained was always lower than 3%. Channiwala's correlation always led to an intermediate value among those obtained by the others.

Table 1
Characterization of samples.

	S0	SK	SNa	SKW	SNaW
C (%)	47.6	21.9	26.5	44.2	44.5
H (%)	6.08	2.7	3.1	5.5	5.7
O (%)*	44.7	22.8	26.8	43.6	44.5
N (%)	0.21	0.1	0.12	0.25	0.23
Moisture (%)	3.8	8.4	8.3	7.0	7.4
Ash (%)	1.4	52.5	43.5	6.5	5.1
Volatile matter (%)	76.7	27.4	24.9	68.2	68.7
Fixed carbon (%)	18.1	11.7	23.2	18.3	18.8
$HHV_{dry\ basis}$ (MJ kg^{-1})	19.1	7.4	9.2	17.3	17.5
K	1997 ppm	31.0%	1115 ppm	4.2%	850 ppm
Na	10.4 ppm	4.8 ppm	24.5%	2.0 ppm	2.3%

(* by difference)

2.3.3. Thermogravimetric analysis (TGA)

TGA was conducted in a Thermal Analyzer Instruments (METTLER TOLEDO model TGA / DSC1 STAR System) operating at a heating rate of 20 °C min^{-1} from 25 °C to 700 °C in a silicon oxide sample vial with N_2 flux of 20 mL min^{-1}. The TGA was conducted with approximately 6 mg of sample.

2.3.4. Infrared spectroscopy (FTIR)

The thermogravimetric analyzer was coupled to the FTIR spectrophotometer (FTIR BRUKER TENSOR 27) to investigate the evolution of gaseous products on-line, providing information on the different functional groups generated during the slow pyrolysis process. The TG was connected to FTIR by a transfer line heated to 230 °C, the same temperature as the FTIR gas cell, to minimize condensation of volatiles. IR spectrum bands in the range 600–4000 cm^{-1} were measured. The time difference between FTIR and TG is about 3 min, due to the time required for the carrier gas flow to fill the volume of the spectrometer cell.

2.3.5. Pyrolysis EGA/Py-GC/MS

Analytical pyrolysis was conducted on a Multi-Shot-Pyrolyzer EGA/Py 3030D connected on-line to a gas chromatograph (model Agilent 6890B) with mass spectrometer detector (model Agilent 5973 MSD). The pyrolizer consists of a quartz reactor surrounded by a ceramic furnace capable of heating up to 1050 °C. A weighed amount of sample (around 0.1 mg) is placed into a sample holder which goes into the quartz reactor by free fall. The reactor is previously heated at the operation temperature selected and a flash pyrolysis of the sample takes place. Volatiles evolved during 12 s are conducted into the GC through an interface heated to 300 °C. A mass spectrometer acts as detector.

Pyrolysis tests were carried out under four different temperatures in the range 400–800 °C. The chromatography column used was HP-5MS UI (30 m x 250 μm x 0.25 μm) and the operation conditions selected were: helium flow in the column: 2 mL min^{-1}, injection mode: split (1:50), injector temperature: 280 °C, initial furnace temperature: 45 °C for 5 min, heating rate: 12 °Cmin^{-1} and final temperature: 285 °C for 10 min.

3. Results and discussion

3.1. Sample characterization

The samples studied were characterized by analyzing different parameters. The results are shown in Table 1.

The results shown for sample S0 agree with others found previously in the literature. Thus, different authors (Munir et al., 2009; Rocha et al., 2015; Nunes et al., 2020) analyze the elemental composition of bagasse samples from different origins (Pakistan, Brazil, Costa Rica). The percentages reported of C, H, O and N are in the ranges 38–48, 3.4–7.4, 41–52 and 0.1–1.7%, respectively. Díaz (2008) shows the elemental

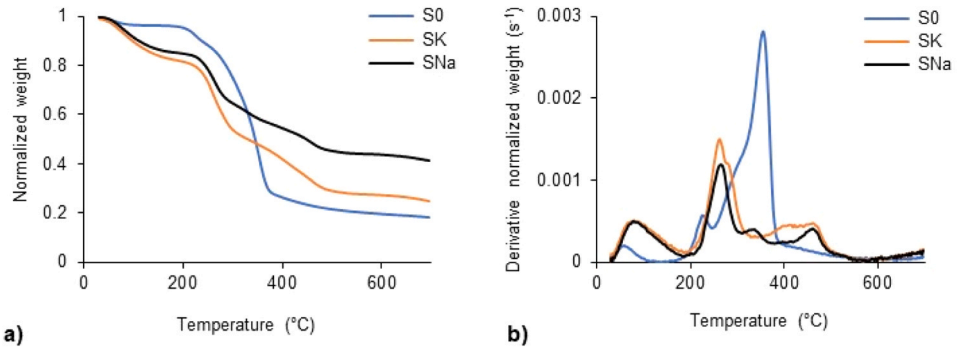

Fig. 1. TG (a) and DTG (b) curves of bagasse, bagasse impregnated with KOH and bagasse impregnated with NaOH (curves normalized to ash-free basis).

composition of 3 bagasse samples from Ecuador, as that one used in the present work. In that case, the values reported were around 47% C, 5% H, 42% O and 0.35% N, very close to those shown in Table 1. About the proximal analysis, the ash content reported varies between 1% and 12%, being in the range 1–5% in most of the cases, while volatiles and fixed carbon percentages are around 71–83% and 13–17%, respectively. The high heating values found for bagasse samples range between 11.6 and 18.8 MJ kg^{-1}. According to this information, the results obtained for S0 are consistent with data found in previous references for similar raw materials.

Soomro et al. (2023) published the chemical composition of sugarcane bagasse ash from different countries, SiO_2 being the major component (23–78%). Low values were reported for Na_2O (from 0% to 1.36%) while K_2O content can reach up to 12.8%, especially in ashes of samples from Brazil. By considering these values and the ash content of the bagasse in the present study, these percentages would imply a maximum Na and K content in the sample of 141 and 1487 ppm, respectively, which is consistent with the results shown in Table 1. Obviously, these values are modified with the alkaline treatments. The significant increase in the ash content of the alkaline samples reduces drastically the percentage of volatiles and fixed carbon. Obviously, when these values are expressed based on the organic content of the sample (i.e., dry ash-free basis), the percentage of fixed carbon (fixed carbon/(volatiles+fixed carbon)) increases in SK and SNa, significantly (29.9% and 48.2%, respectively), while the percentages of volatiles (volatiles/(volatiles+fixed carbon)) decreases. According to these results, the incorporation of NaOH into the bagasse generates more char than KOH does. One of the aspects that may influence this result is that KOH is a more powerful activating agent, reacting with carbon to generate H_2 or CO_2 (Martínez-Escandell et al., 2013), therefore obtaining less char.

The alkaline treatment does not imply any risk either in the process or in the pyrolytic products generated. The volatiles evolved do not need any post-treatment since the alkalis remain as inorganic components in the carbon residue. The presence of these cations (mainly K^+) in the residue can provide two interesting applications:

a) addition of carbon as soil amendment, especially in acidic soils, without the necessity of eliminating K^+ since it is a fertilizer;
b) carbon activation due to the presence of chemical activating agents. As said previously, KOH is a potent agent whose activation mechanism has been well-studied (Martinez-Escandell et al., 2013). The activating agents can be removed from the activated carbon by washing the product with acid solution and distilled water (Ruiz Beviá et al., 1984; Williams et al., 2022).

In any case, the operating parameters of the pyrolysis process (and activation, if applicable) would have to be controlled.

3.2. TGA analysis

Fig. 1 presents the results of the mass loss curve (TG) and the derivative of the mass loss vs. temperature (DTG) for untreated bagasse residue (S0), bagasse treated with potassium hydroxide (SK) and bagasse treated with sodium hydroxide (SNa), at a heating rate of 20 °C min^{-1}. The curves have been normalized to ash-free basis.

For sample S0, 4 different processes can be observed, which are clearly identified in the DTG curve. The first one begins at around 170 °C and shows its maximum decomposition rate at 230 °C. This peak could be attributed to the pyrolysis of total soluble sugar, mainly sucrose, present in the sugarcane bagasse and whose content can vary depending on the sugarcane plant and the obtention methods of the bagasse (Wang et al., 2022b). Thus, for example, Motaung and Anandjiwala (2015) worked with sugarcane bagasse -supplied by a farm in South Africa- and no DTG peak was observed in that temperature range. The rest of the curve follows the typical pattern of the lignocellulosic biomass decomposition, in which the highest emission of volatiles occurs between 250 and 400 °C, a range where the decompositions of hemicellulose, cellulose and lignin take place and overlap. Thus, a shoulder can be distinguished in the range 250–310 °C, which mainly corresponds to the decomposition of hemicellulose, while the main DTG peak is placed at 355 °C, mostly identified with the cellulose decomposition process. Lignin degradation is a low rate process that covers a wide range of temperatures (250 – 600 °C, approximately). At temperatures higher than 400 °C, the main process occurring is associated with the aromatization of lignin fraction, which leads to a low weight loss (Fisher et al., 2002; Ounas et al., 2011).

Samples SK and SNa follow a different thermal behavior from S0. On one hand, a significant increase of char compared to untreated sample is reached (24,6% in SK and 41.1% in SNa vs. 18.3% in S0, expressed in ash-free basis). On the other, it is observed that the shape of the TG and DTG curves has been highly modified and their decomposition takes place over a wider temperature range, starting at around 200 °C and being extended up to 500 °C. The main DTG peak placed at 355 °C in sample S0 is found at 265 °C in these samples. Two regions can be distinguished in these curves: one is centered in the range 200–300 °C and the other in the range 300–500 °C. The decomposition process takes place, approximately, 50% in each range.

These thermogravimetric curves could be the result of the addition of two effects: 1) modification of the lignocellulosic structure of the bagasse due to the alkaline treatment; 2) catalytic effect on the bagasse decomposition, due to the presence of K^+ and Na^+ in the sample during the pyrolytic process.

About the possibility of changes in the biomass composition due to the treatment, Bartos et al. (2020) observed a weight loss in the sugarcane bagasse fibers during their experiments, where this type of fibers was treated with NaOH solutions (1–40 wt%) at room temperature for 1 h and then washed until pH neutral. These authors reported a decrease in the hemicellulose and lignin contents by increasing NaOH

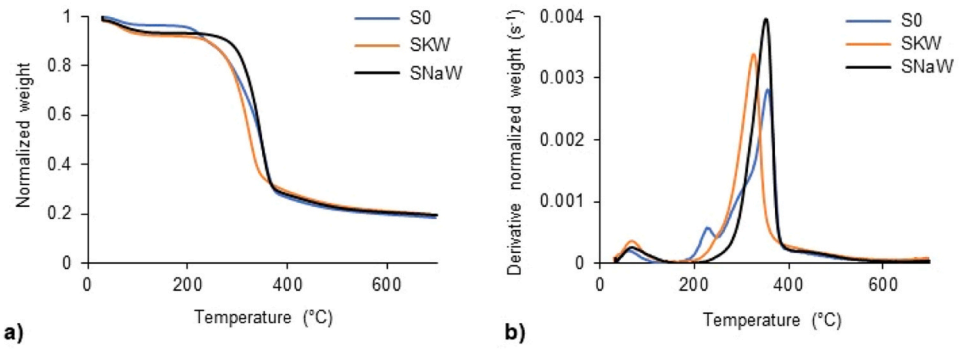

Fig. 2. TG (a) and DTG (b) curves of bagasse and washed treated bagasse (curves normalized to ash-free basis).

concentration, while cellulose showed a maximum, being also reduced its content at large alkali concentrations.

About the catalytic effect due to the presence of hydroxides in the structure, it is known that cations such as K^+ or Na^+ can catalyze the degradation process of biomass favoring a degradation mechanism that leads to its fragmentation into smaller molecules and char formation over other decomposition ways such as depolymerization with monomer formation (Sebestyén et al., 2013). In fact, it can be observed in the TG curves that the alkaline treatment has increased significantly the residue (char) yield, which is coherent with the idea exposed about the effect of alkaline ions in enhancing the charring reaction.

In order to deduce which effect could have more influence on the results obtained, samples SK and SNa were washed to remove the ions. Fig. 2 shows TG and DTG curves for samples SKW and SNaW compared to S0. In the washed samples, the ions previously added to the bagasse have been removed and, according to the ash measurements, only an ash content slightly higher than that of the untreated sample has remained. In this way, the catalytic effect that could occur in samples SK y SNa has been minimized and the effect of the structure modification plays now a greater role in the results obtained.

As can be seen, although the decomposition of SKW and SNaW differs from that of the original bagasse, they show much more similarities with S0 than with the curves of the alkaline samples (SK and SNa).

In washed samples, the curves are simpler and fewer processes are distinguished. A main process is detected, similar to that associated with the cellulose decomposition in S0, and a minor process, at higher temperatures, corresponding to the pyrolysis of the remaining lignin. The DTG peak associated with the sucrose decomposition is not observed in either of the two samples. This fact agrees with the idea that the peak was associated with soluble sugars, which would have been removed in the washing process. The shoulder corresponding to the hemicellulose degradation is slightly detected in SKW and it is not distinguished in SNaW. It could be due to a high percentage of hemicellulose that has been solubilized with the treatment. However, Sebestyén et al. (2011) reached similar results in their experiments studying the thermal decomposition of hemp and verified that the hemicellulose content had not changed significantly in the sample after the alkaline treatment (KOH or NaOH, 1–2%). Thus, they suggested that its side groups, such as acetyl groups, had been removed, increasing the thermal stability of the hemicellulose which decomposed at higher temperatures, in a similar range to cellulose.

By comparing the temperature values of the DTG peaks, it is observed that in the case of washed samples, this value is lower than that of the original bagasse although very close to it: 355 °C for S0 vs. 353 °C for SNaW and 325 °C for SKW. These differences could be explained by the slight increment in ash content in washed samples. In the case of SK and SNa, the value of this temperature was around 265 °C in both cases. The presence of some alkali remaining in SKW and SNaW is also observed by the increase in the carbonaceous residue in contrast to S0, although it is much lower than that generated with alkaline samples.

According to these results, the decrease in the temperature of the DTG peak as well as the shape of the thermogravimetric curves in samples SNa and SK are due to the catalytic effect of the alkali ions present in the samples, rather than to previous changes in the bagasse structure as a consequence of the pretreatment performed. The impregnation process at room temperature and the sample drying at 100 °C have only partially modified the hemicellulose fraction of the bagasse, without causing mechanism changes in the decomposition of the sample.

3.2.1. *Kinetic study*

Thermogravimetric analysis is a common tool for the development of kinetic models. The greater the amount of data used in the development of the model, the greater the reliability of the parameters obtained. For this reason, the kinetic models proposed from TGA data usually fit, simultaneously, thermogravimetric curves obtained at different heating rates (García and Font, 2004; Vyazovkin et al., 2011; Bañón et al., 2016). Although the main objective of this work is not to obtain kinetic parameters of the decomposition processes studied, a simple model has been developed, adjusting the experimental TG and DTG curves obtained for each sample, at 20 °C min^{-1}, in order to highlight similarities and differences between their decomposition processes.

Thus, a model of independent reactions has been proposed, where each reaction corresponds to the decomposition process of the different fractions that make up the biomass. A similar model has been used previously to reproduce decomposition processes of different biomasses, leading to satisfactory results (Esperanza et al., 1999; Hirunpraditkoon and García, 2009; Londoño-Larrea et al., 2022).

The model reactions can be represented as:

$$w_{0i}\ W_i \rightarrow v_i\ V_i + (w_{0i}\text{-}v_i)\ C_i \quad (2)$$

where the subscript *i* refers to the different fractions that form the biomass; *W*, *V* and *C* correspond to the biomass fraction, the volatiles evolved and the residue generated in the process, respectively; w_0 is the initial mass fraction and *v* is the maximum mass fraction of the volatiles evolved.

The decomposition equation for each fraction can be written as:

$$-dwi/dt = k_{oi}\ exp(-Ei/RT)wi^n \quad (3)$$

where *w* is the mass fraction of *W* at each time *t* and temperature *T*, *n* is the reaction order and the kinetic constant of the reaction has been expressed according to the Arrhenius equation, where *ko* is the pre-exponential factor and *E* the activation energy.

According to the model proposed, at each time, the percentage of undecomposed biomass ($w_{calc,t}$) is calculated as the sum of the mass fractions of each biomass component at time *t*. Similarly, the variation of mass with time $\left(\left(\frac{dw}{dt}\right)_{calc,t}\right)$ is calculated as the sum of the variations of the different fractions considered.

Parameters *woi*, *koi*, *Ei* and *ni* have been fitted by minimizing the

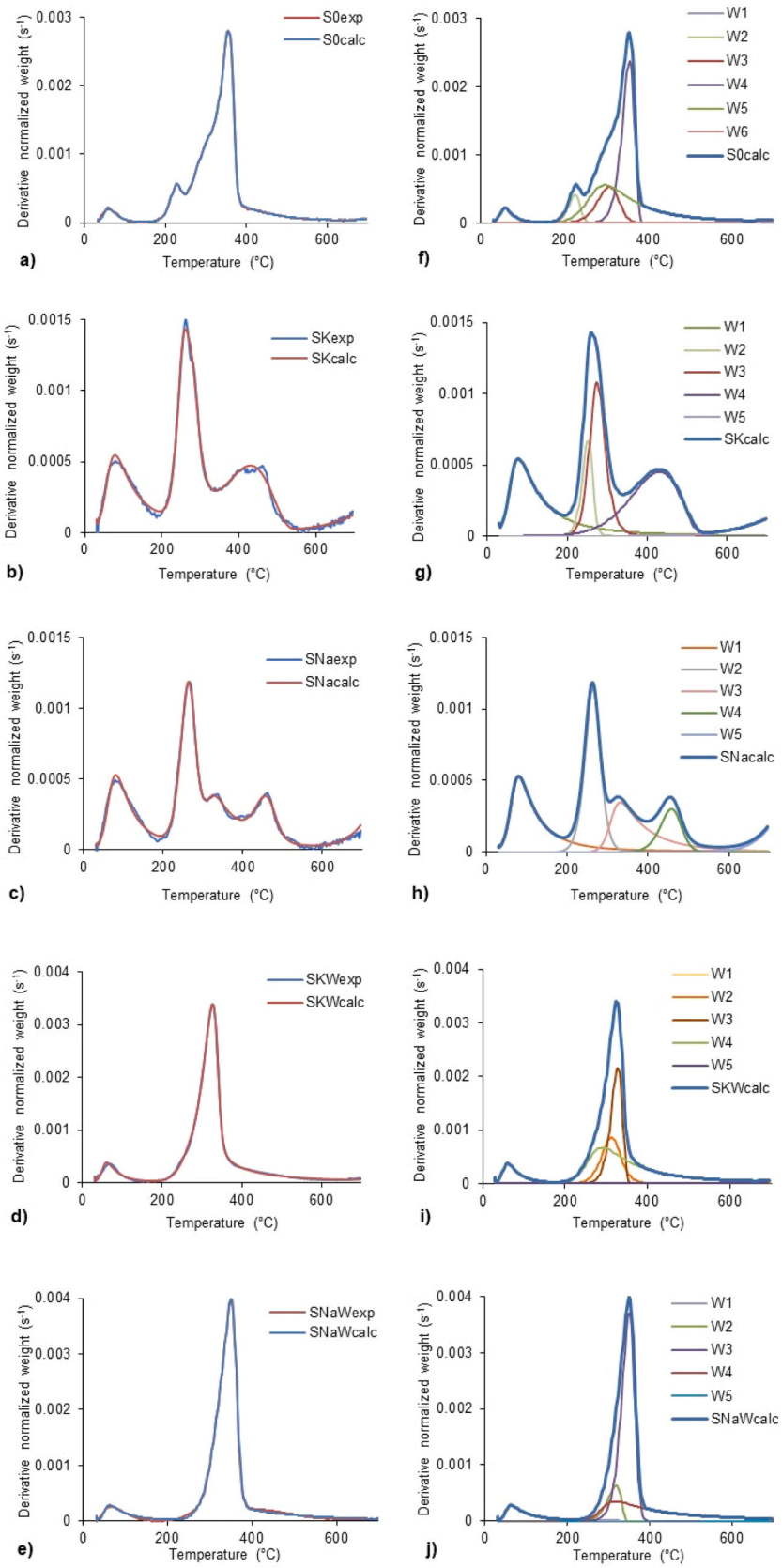

Fig. 3. (a-e) Comparison between experimental and calculated DTG curves; (f-j) Deconvolution of the DTG curves (curves normalized to ash-free basis).

Table 2
Fitting parameters for S0.

	W1	W2	W3	W4	W5	W6
w_0 (%)	3.9	4.9	11.6	30.3	32.3	17.0
ko (s^{-1})	$1.70{\cdot}10^{19}$	$2.53{\cdot}10^{15}$	$5.15{\cdot}10^{8}$	$1.44{\cdot}10^{16}$	$1.26{\cdot}10^{7}$	$1.55{\cdot}10^{7}$
E ($kJmol^{-1}$)	129.2	161.6	117.4	213.8	99.8	202.4
n	4.2	1.3	1.3	1.1	4.7	0.43
$T_{max,\ DTG}$ (°C)	59.8	225.5	307.3	355.7	298.3	700
OF	$2.20{\cdot}10^{-4}$					

Table 3
Fitting parameters for SK.

	W1	W2	W3	W4	W5
w_0 (%)	23.6	7.6	18.7	23.2	26.8
ko (s^{-1})	$8.80{\cdot}10^{9}$	$3.22{\cdot}10^{17}$	$3.57{\cdot}10^{15}$	47	166
E ($kJmol^{-1}$)	77.6	190.9	179.7	54.4	102.0
n	7.0	1.4	2.2	0.82	1.7
$T_{max,\ DTG}$ (°C)	76.7	253.0	274.0	430.9	700
OF	$2.04{\cdot}10^{-3}$				

Table 4
Fitting parameters for SNa.

	W1	W2	W3	W4	W5
w_0 (%)	17.4	18.9	14.4	6.8	42.4
ko (s^{-1})	$1.10{\cdot}10^{11}$	$5.45{\cdot}10^{13}$	$1.96{\cdot}10^{17}$	$1.91{\cdot}10^{12}$	$2.95{\cdot}10^{6}$
E ($kJmol^{-1}$)	85.6	157.8	219.8	197.4	182.3
n	5.6	1.7	7.1	1.4	-0.99
$T_{max,\ DTG}$ (°C)	79.6	265.0	331.8	458.0	700
OF	$1.39{\cdot}10^{-3}$				

Table 5
Fitting parameters for SKW.

	W1	W2	W3	W4	W5
w_0 (%)	8.5	15.5	22.9	36.6	16.4
ko (s^{-1})	$1.87{\cdot}10^{19}$	$1.57{\cdot}10^{12}$	$2.86{\cdot}10^{17}$	$1.39{\cdot}10^{9}$	$1.73{\cdot}10^{7}$
E ($kJmol^{-1}$)	128.4	155.4	217.9	119.3	206.1
n	5.5	1.8	1.2	6.5	0.92
$T_{max,\ DTG}$ (°C)	61.7	311.0	327.9	290.7	700
OF	$1.53{\cdot}10^{-3}$				

Table 6
Fitting parameters for SNaW.

	W1	W2	W3	W4	W5
w_0 (%)	8.0	7.9	45.2	25.1	13.8
ko (s^{-1})	$2.51{\cdot}10^{19}$	$7.71{\cdot}10^{11}$	$8.07{\cdot}10^{15}$	$9.14{\cdot}10^{11}$	$3.19{\cdot}10^{5}$
E ($kJmol^{-1}$)	130.2	153.1	208.5	156.5	206.2
n	8	0.86	1.2	11.1	0.87
$T_{max,\ DTG}$ (°C)	61.9	318.9	349.3	315.5	700
OF	$4.25{\cdot}10^{-3}$				

following objective function:

$$OF = \sum_{t}\left[\left(w_{\exp,t} - w_{calc,t}\right)^2 + 10^4\left(\left(\frac{dw}{dt}\right)_{\exp,t} - \left(\frac{dw}{dt}\right)_{calc,t}\right)^2\right] \quad (4)$$

where $w_{exp,t}$ and $\left(\frac{dw}{dt}\right)_{\exp,t}$ are the values from experimental TG and DTG curves, at any time. The difference corresponding to DTG values has been multiplied by a factor to balance both terms (TG and DTG values) in the fitting.

The model proposed perfectly fits the TG curves, without distinction between experimental and calculated data, and reproduces the DTG curves with great similarity. Fig. 3 compares the experimental and calculated DTG curves (ash-free basis) for each sample. To distinguish the processes involved in their decomposition, Fig. 3 also includes the deconvolution of the DTG curve, according to the model considered.

As can be seen, a very good fit has been obtained for each sample. For the correct adjustment throughout the temperature range studied, it has been necessary to consider the decomposition of 5 or 6 fractions. By observing the range of temperatures for each fraction in the untreated bagasse (Fig. 3f), it is possible to associate each one with one of the components of this biomass. Thus, W1, whose decomposition takes place at temperatures below 100 °C, corresponds to the humidity content of the sample and W2 would be associated with the decomposition of the sucrose percentage that has been mentioned previously. W3 and W4 would correspond mainly to the hemicellulose and cellulose fraction, while the wide range of decomposition temperature of W5 allows it to be associated with the lignin fraction. It has been necessary to include the fraction W6 to adjust the small change in the slope of the DTG curve at temperatures above 600 °C. This fraction remains constant up to that temperature, where a slight decomposition begins. Any attempt to avoid this fraction in the adjustment prevented fitting that part of the curve.

These fractions, except that corresponding to the sucrose content, can be identified again in washed treated samples (Fig. 3i-j). The influence of alkaline catalyst on SK and SNa makes it more difficult to relate the fractions obtained with the hemicellulose, cellulose, and lignin content of the sample (Fig. 3g-h), once the fractions and their decomposition processes have been modified by the presence of alkalis. Despite this, W2 and W3 in SK could be related to hemicellulose and cellulose fractions, respectively. In the case of SNa, both fractions could be overlapping and represented only by W2.

Tables 2–6 show the values obtained for the fitting parameters (*woi*, *koi*, *Ei* and *ni*). The value of the maximum decomposition rate temperature ($T_{max,\ DTG}$) for the different adjusted fractions has also been included.

In all samples, W1 corresponds to the moisture content. As was already observed in DTG curves, this content is higher in the SK and SNa samples. Probably, given the hygroscopic nature of KOH and NaOH, a more aggressive drying treatment would have been needed to reduce their water content. The last fraction (W6 in S0 and W5 in the rest of the samples) corresponds to the constant fraction that decomposes at high temperatures. That is why the value of $T_{max,\ DTG}$ is always 700 °C. The value of w_0 for this fraction coincides with the value of the residue reached in each sample. Since the pyrolysis of cellulose hardly generates carbon residue and the char generated mainly comes from the decomposition of lignin and hemicellulose (Yu et al., 2017), the value of w_{06} in S0 can be assumed to be part of lignin and hemicellulose, which would increase their percentages in the bagasse (w_{o3} and w_{o5}).

When the model was applied to the TG and DTG curves including the ashes of the samples, results very similar to those shown in Tables 2–6 were obtained, except for the value of w_{06} in S0 (or w_{05} in the rest of the samples), since this fraction included, in addition to the carbon residue, the value of the sample ashes.

The kinetic parameters obtained for W3, W4 and W5 in S0 have been compared with kinetic parameters for decomposition processes of hemicellulose, cellulose and lignin, reported previously in literature. Rueda-Ordóñez and Tannous (2017) collected activation energy and pre-exponential factor data for the decomposition of these 3 components provided by different researchers, studying different biomasses.

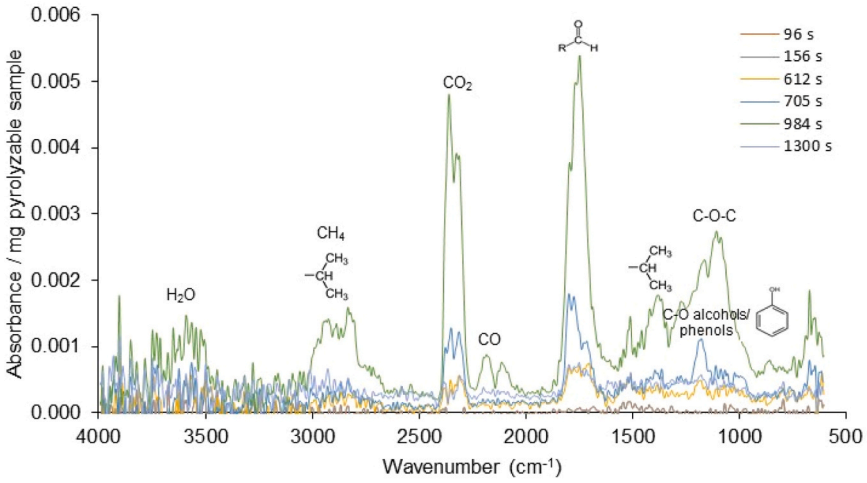

Fig. 4. FTIR spectra of the volatiles evolved from the slow pyrolysis of bagasse at different times.

According to this review, the value of E_a (kJ mol^{-1}) for hemicellulose is concentrated between 100 and 200 and 125–225 for cellulose, with values of k_0 (s^{-1}) around 10^6 - 10^{18} in the first case and for 10^8 - 10^{17} in the second. Lignin showed the lowest values, between 50 and 150 kJ mol^{-1} for E_a and 10–10^9 s^{-1} for k_0. As can be seen, the values shown in Table 2 fit in these ranges perfectly. These authors also calculated the kinetic parameters for the decomposition of hemicellulose, cellulose and lignin contained in the sugarcane bagasse. The values obtained were E_a (kJ mol^{-1}) 124, 208 and 133, respectively, with k_0 (s^{-1}) values of 10^9, 10^{15} and 10^6. García-Pérez et al. (2001), working with similar raw material, deduced E_a values (kJ mol^{-1}) of 105, 235 and 26 for the 3 components. On the other hand, Ounas et al. (2011) reported values between 168 and 180 kJ mol^{-1} for the activation energy of hemicellulose contained in bagasse and 231–240 kJ mol^{-1} for cellulose, without including values for the decomposition of the lignin fraction.

According to these results, the data reported in the present paper are consistent with the information found in the literature and can serve as a basis for a more robust model that fits different thermogravimetric curves generated at different heating rates.

3.3. FTIR analysis

An FTIR spectrophotometer was connected on-line to the TGA equipment to obtain information about the main functional groups of the volatiles generated in the experiments.

Fig. 4 shows the evolution of FTIR spectra for the untreated sample as a function of time. As can be seen, the signals obtained are more intense at 984 s, which corresponds to the temperature of the maximum decomposition rate in the DTG curve (355 °C). It must be taken into account that the transfer line is at 230 °C, so the condensation of heavy products could occur. Despite that, different regions can be distinguished in this spectrum. The presence of water is deduced by the bands in the 4000–3500 cm^{-1} range that correspond to O-H stretching vibrations and those around 1500 cm^{-1} corresponding to O-H bending vibrations (Marcilla et al., 2009). A sharp signal at 2349 cm^{-1}, corresponding to asymmetrical stretching vibrations in O═C═O, characteristic of CO_2, is clearly observed in the spectrum, as well as the bands detected at around 2180–2100 cm^{-1}, associated with CO formation (Gómez-Siurana et al., 2013). The strong absorption band observed in the region 1870–1540 cm^{-1} is associated with the C═O stretch, which can be assigned to aldehydes, ketones, acids and esters (Marcilla et al., 2009).

Signals located at around 2970–2820 cm^{-1} are characteristics of the C-H stretch and those in 1485–1370 cm^{-1} of C-H bend in methyl and methylene groups, indicating the presence of alkanes or alkyl substituents (Gómez-Siurana et al., 2013). Chen et al. (2019) associated signals in the region 3050–2650 cm^{-1} specifically with methane caused

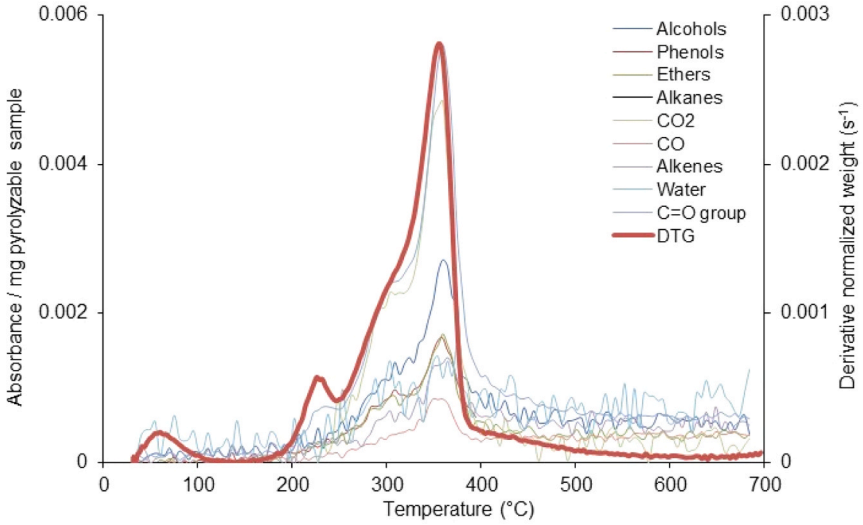

Fig. 5. Comparison between DTG and FTIR analyses of the bagasse.

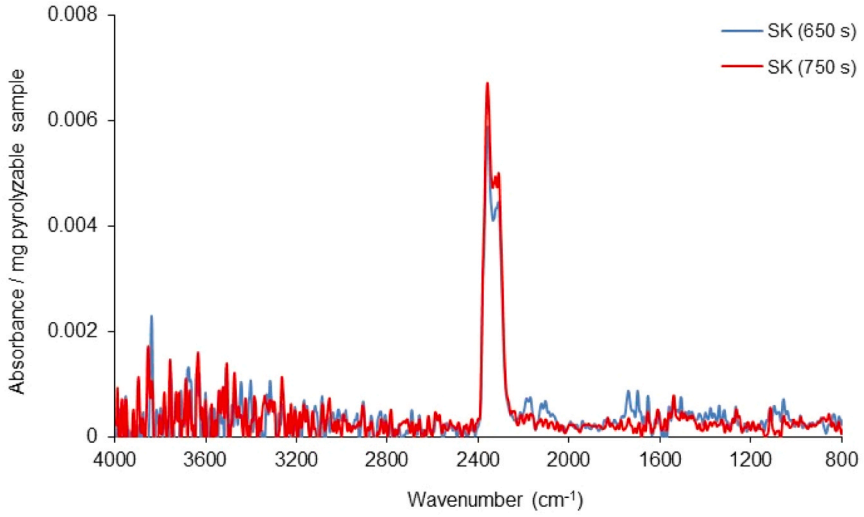

Fig. 6. FTIR spectra of the volatiles evolved from the slow pyrolysis of KOH impregnated bagasse at two different times.

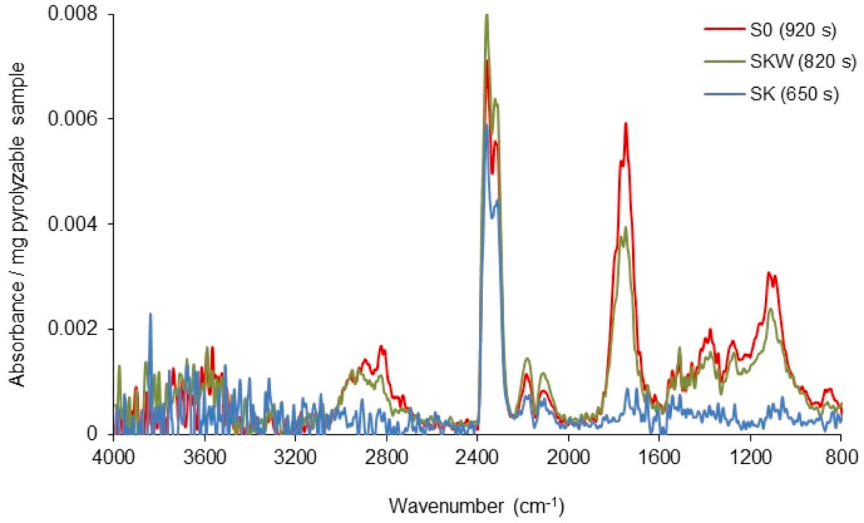

Fig. 7. Comparison of FTIR spectra of the volatiles evolved from the thermal decomposition of bagasse, KOH impregnated bagasse and washed KOH sample.

by the breakage of methoxy, methylene and methyl groups.

In the region 1500–1000 cm^{-1}, different overlapped bands associated with different origins are detected. Besides signals related to the presence of water and alkanes commented on previously, other functional groups are associated with the bands in this spectrum region. Thus, signals at around 1508 cm^{-1}, 1108 cm^{-1}, 1032 cm^{-1} could correspond to aromatic rings. This idea is validated by the presence of a clear and isolated band at 846 cm^{-1} which is associated with aromatic C-H out of plane bending (Zhuang et al., 2020). The stretching vibrations of C-O-C bond, corresponding to ethers, produce a band in the 1200–900 cm^{-1} region (Marcilla et al., 2009). These signals can be overlapped with those corresponding to C-O stretch in alcohols and phenols located in the range 1200–1050 cm^{-1} (Gómez-Siurana et al., 2013).

Yang et al. (2007) studied the thermal decomposition of the three major components of the biomass (hemicellulose, cellulose and lignin) independently, by a TGA-FTIR system. Absorption bands corresponding to H_2O, CO_2, CO, CH_4, C═O and C-O-C were detected, the signal intensity being higher in CO_2 and C═O. All the compounds and functional groups were observed in the pyrolysis of the three components, varying the absorbance intensity from one to another. According to their results, hemicellulose is the one that contributes the most to the emission of CO_2 and CO, (formed by the cracking of carbonyl, carboxyl and O-acetyl groups (Chen et al., 2019)), lignin to that of CH_4 (probably due to the decomposition of methoxyl-O-CH_3 groups) and cellulose to water (caused by cleavage of hydroxyl groups (Chen et al., 2019)). Regarding the emission of organic compounds with C═O and C-O-C groups, both hemicellulose and cellulose contribute significantly (from the ring-opening reactions (Chen et al., 2019)), the contribution of lignin being almost negligible.

Fig. 5 shows the sugarcane bagasse DTG graph as well as the evolution with temperature of the intensity of several signals associated with different functional groups. As can be observed, both types of graphs fit perfectly.

Fig. 6 compares the IR spectra of SK at two different times, selecting those in which the evolution of the volatiles is maximum, corresponding to 242 and 275 °C. As can be seen, the spectra are highly different from those of the untreated sample and only the absorption bands associated with H_2O, CO and CO_2 are comparable in intensity to those of bagasse; those corresponding to C═O group, phenols and ethers have been drastically reduced. It is worth mentioning that CO_2 reaches its maximum at higher temperature than the rest of products, since CO_2 signal is the only one that increases from 650 to 750 s.

Fig. 7 compares the IR spectra of the original bagasse with those of

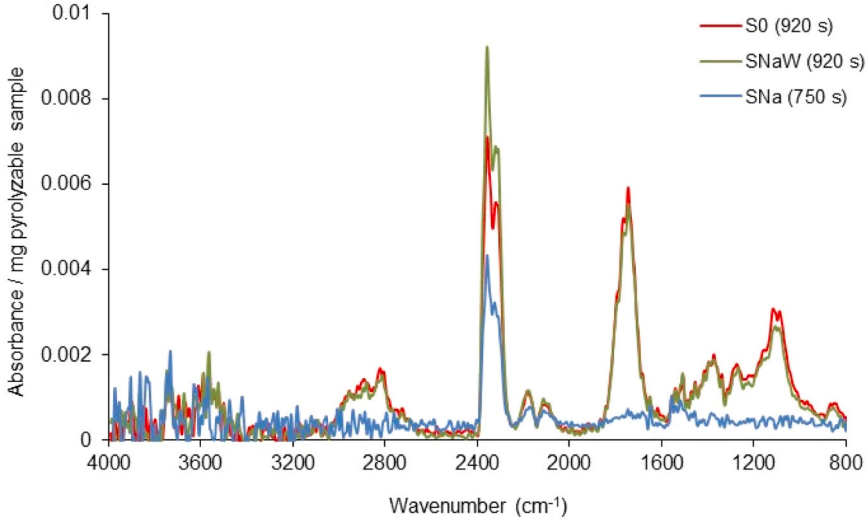

Fig. 8. Comparison of FTIR spectra of the volatiles evolved from the thermal decomposition of bagasse, NaOH impregnated bagasse and washed NaOH sample.

Table 7
Main FTIR signals.

Wavenumber (cm^{-1})	assignment	Tmax (°C)				
		S0	SK	SNa	SKW	SNaw
2349	vibrations in O═C═O (CO_2)	355	275	310	312	355
2180–2100	CO		242	275		
1870–1540	C═O stretch (aldehydes, ketones, acids and esters)		-	-		
2970–2820	C-H stretch		-	-		
1485–1370	C-H bend (methyl and methylene groups)		-	-		
1508, 1108, 1032	aromatic rings		242	275		
1200–900	vibrations of C-O-C bond (ethers)		-	-		
1200–1050	C-O stretch (alcohols and phenols)		-	-		

SK and SKW. In each case, it has been selected the spectra corresponding to the time of maximum evolution of volatiles, so each one corresponds to a different time (temperature), which agrees with the TG/DTG curves (Figs. 1 and 2). Similar to the information deduced from the TG study, the decomposition of the washed-treated sample is much more similar to that of the original bagasse than to the decomposition of the treated one. As can be seen, the functional groups detected in S0 and SKW are the same, only modifying the signal intensities. The comparison of spectra clearly reveals a change in the decomposition mechanism of the SK sample compared to the S0, generating much less volatiles but high CO_2 yields while, in the SKW sample, the differences observed in the absorption band intensity are due to a change in the biomass structure, rather than changes in the decomposition mechanism. As commented on previously, the alkaline treatment followed by washing may have solubilized part of the hemicellulose and lignin, or at least part of their side chains (such as the acetyl groups in the hemicellulose), thus reducing the yield of some products, especially the carbonyl-containing components.

Similar conclusions can be reached by analyzing the effect of NaOH. Fig. 8 compares spectra from S0, SNa and SNaW. In this case, the temperature reduction of the decomposition process has been lower than with KOH, and S0 and SNaW spectra have been compared at the same time. The catalytic effect of alkaline ions is shown again in the treated

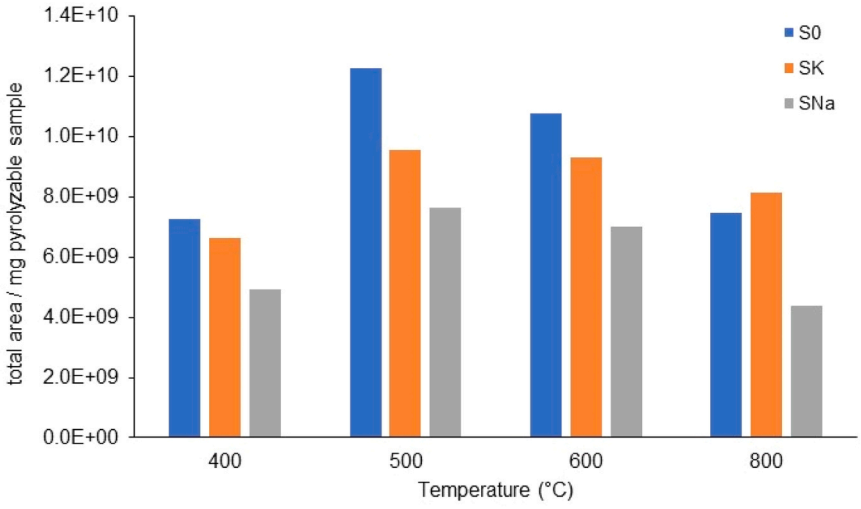

Fig. 9. Total chromatographic area of the volatiles evolved from the flash pyrolysis of bagasse, KOH impregnated bagasse and NaOH impregnated bagasse, as a function of temperature.

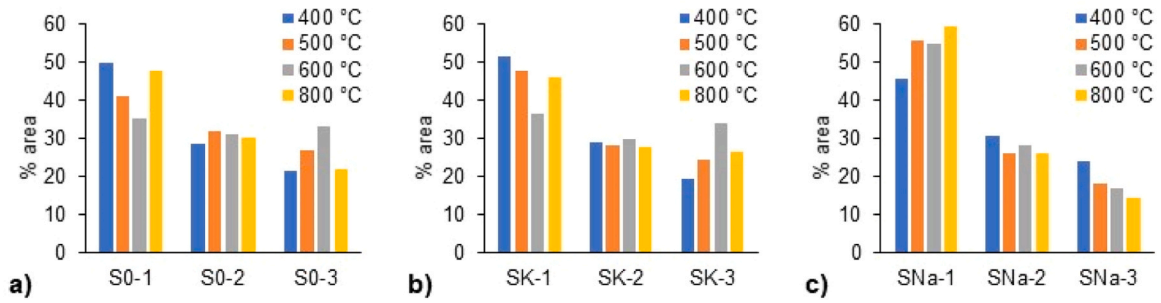

Fig. 10. Percentage of the chromatographic area corresponding to the 3 established groups as a function of temperature: a) bagasse; b) KOH impregnated bagasse; c) NaOH impregnated bagasse.

sample, reducing the volatiles evolved; only signals associated with CO_2, CO and H_2O are especially remarkable. TG and FTIR results support the idea that alkaline ions favor the carbon oxides and charring reactions against the formation of heavier volatile molecules (Sebestyén et al., 2011). The washed sample shows a very similar spectrum to the untreated one, slightly modifying the intensity of the absorption bands, increasing that of CO_2 and reducing those corresponding to the other functional groups.

Table 7 summarizes the main FTIR signals detected in each sample, as well as the temperature where the maximum intensity of the signal has been observed.

3.4. Analytical pyrolysis (Py/EGA-GC/MS)

The samples studied have been subjected to flash pyrolysis, in order to compare the decomposition processes suffered by the samples under different conditions.

3.4.1. Influence of catalysts

Flash pyrolysis of S0, SK and SNa was performed at different temperatures in the range 400–800 °C, in a Py/EGA-GC/MS system.

Fig. 9 shows the values of total normalized area (total GC area/mg pyrolyzable sample) vs. temperature for the samples studied.

As can be seen, the total chromatographic area shows a maximum at around 500 °C, independently of the sample type. The presence of alkaline hydroxides reduces the volatiles area, NaOH being the hydroxide which leads to the lowest one. Despite the difference in the heating rate between both techniques, the result of the flash pyrolysis agrees with the conclusions reached in the thermogravimetric analysis, where it was observed that the thermal degradation of SNa generated a lower percentage of volatiles and higher char yield.

The total area in each chromatogram was divided into 3 groups, according to the retention time in the chromatogram: 1) 1–10 min, corresponding to compounds with a molecular weight lower than 110 (mainly formed by CO_2 and water), 2) 10–16 min, with compounds with a molecular weight in the range 110–180, 3) 16–20 min, with compounds with a molecular weight higher than 180. Fig. 10 compares the area percentage of these groups for each sample at the temperatures studied.

As can be seen, the influence of NaOH and KOH on the bagasse decomposition mechanism is different. In the case of KOH, increasing the temperature from 400 to 600 °C increases the proportion of heavy volatiles compared to light ones. That means that the increase in temperature has favored the thermal decomposition of the solid, generating heavy volatiles. This behavior is similar to that of the untreated sample. Only at 800 °C, the relationship is inverted, and the percentage of light compounds increases compared to the heaviest ones. In the case of NaOH, the product distribution observed is different, since the percentage of the light volatiles increases from low temperature up to 800 °C, while the progressive reduction in the same temperature range is observed for the heavier volatiles. According to these results, the NaOH modifies the decomposition mechanism of the sugarcane bagasse in a greater extent than KOH, clearly favoring the generation of char and volatiles with low molecular weight.

Each one of the chromatograms is formed by more than one hundred peaks, most of them with low area percentages and difficult identification. Fig. 11 shows an example of the chromatograms obtained.

It is not an easy task to quantify the compounds obtained in this type of chromatograms. In this case, it is common to work with values of compound area/g sample as representative of the compound yield or with area percentages as representative of its mass fraction (Sebestyén et al., 2013; Stefanidis et al., 2016; Schmitt et al., 2020; Londoño-Larrea,

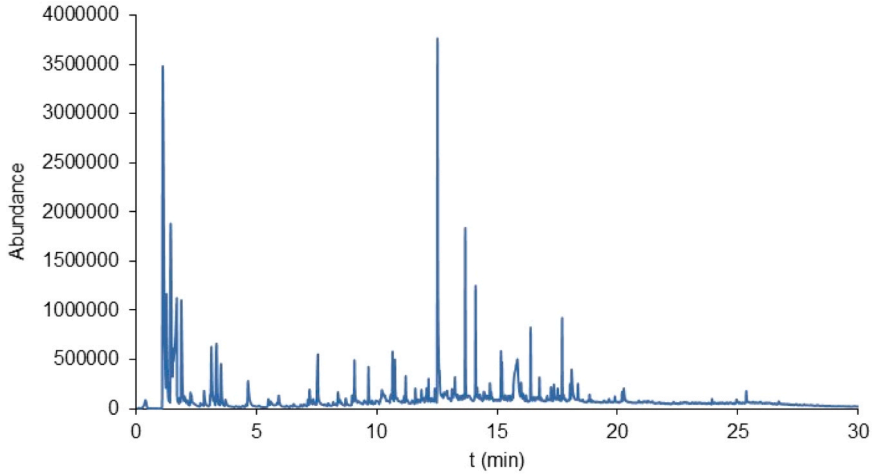

Fig. 11. Example of pyrogram. Pyrolysis of sugarcane bagasse at 500 °C.

Table 8
Percentage of the chromatographic area corresponding to the main volatiles evolved in the flash pyrolysis of the samples at different temperatures (% area).

Compounds	400 S0	400 SK	400 SNa	500 S0	500 SK	500 SNa	600 S0	600 SK	600 SNa	800 S0	800 SK	800 SNa
CO2+agua	10.1	35.1	28.3	8.9	22.9	31.7	9.1	16.7	33.4	11.9	16.7	28.9
acetaldehyde, hydroxy-	2.2	-	-	3.8	-	-	1.6	-	-	-	-	-
acetic acid	9.5	-	-	4. 9	-	-	2.2	-	-	0.92	-	-
2-propanone,1-hydroxy-	3.2	0.65	0.38	2.0	0.94	0.79	1.1	-	-	-	-	-
benzene	-	-	-	-	-	-	-	-	-	2.0	1.4	1.4
toluene	-	-	-	-	-	0.32	-	0.43	0.61	1.5	1.8	1.8
furfural	1.6	-	-	0.83	-	-	1.5	-	-	0.57	-	-
styrene	-	-	-	-	-	-	-	-	0.11	0.62	0.39	0.35
2-hydroxycyclopent-2-en-1-one	1.7	-	-	1.3	-	-	1.2	-	-	-	-	-
phenol	-	1.7	2.3	-	1.5	0.78	-	1.5	0.95	2.2	2.0	1.9
phenol, 2-methoxy	0.48	1.7	2.2	0.63	1.5	1.2	0.37	1.8	0.76	-	-	0.41
phenol, 4-ethyl-	0.30	1.6	1.4	0.38	1.2	1.4	0.35	1.2	3.2	0.82	2.6	3.1
4-vinylphenol	6.6	1.1	2.2	5.1	1.4	1.6	3.3	0.85	1.2	5.3	1.1	2.1
4-vinyl-2-methoxy-phenol	1.9	1.1	1.1	1.9	1.1	0.99	1.4	1.2	1.2	-	-	-
phenol, 2,6-dimethoxy-	1.4	1.3	2.1	1.3	0.87	0.29	0.72	1.2	0.46	-	-	-
levoglucosane	0.89	-	-	3.4	-	-	7.1	-	-	0.71	-	-
2,3,5-trimethoxytoluene	-	1.0	1.1	-	0.50	0.33	-	0.60	0.55	-	-	-
4-((1E)−3-Hydroxy-1-propenyl)−2-methoxyphenol	1.4	-	-	1.1	-	-	1.0	-	-	-	-	-

-: non-detected

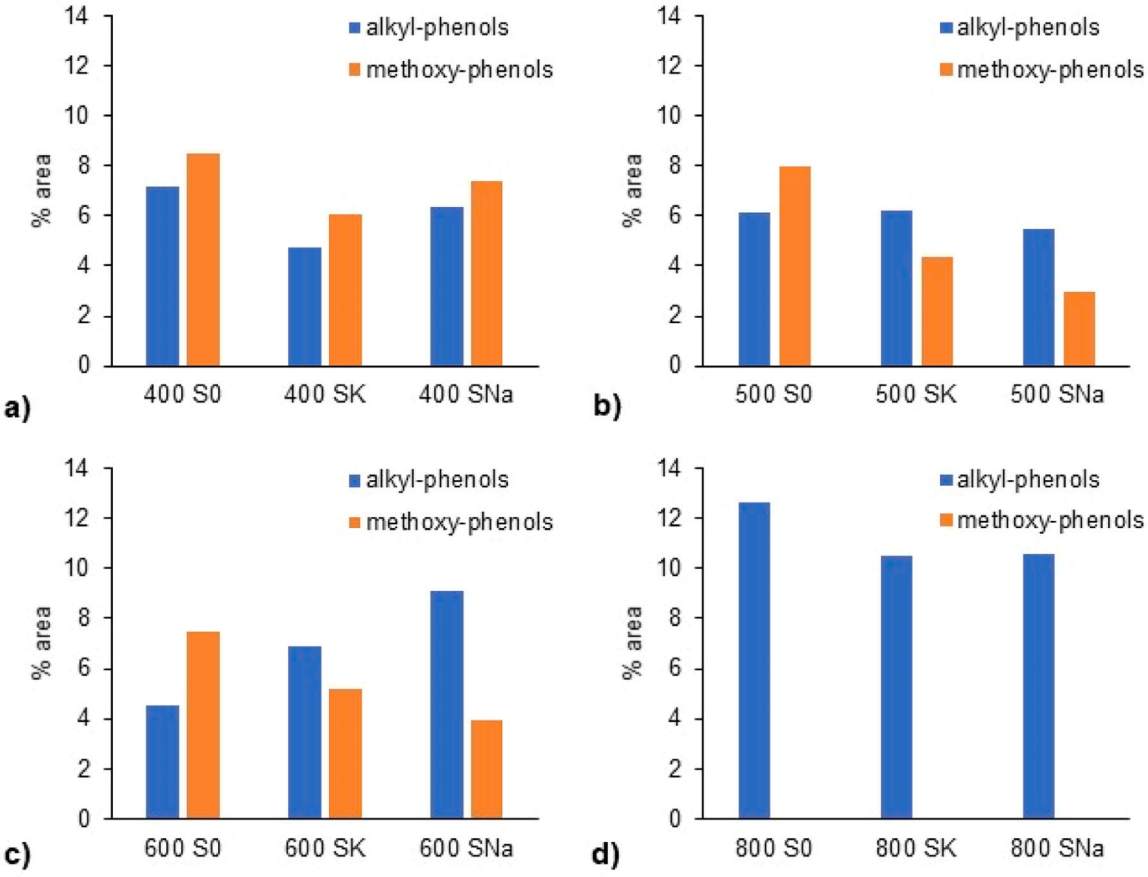

Fig. 12. Percentage of the chromatographic area corresponding to the alkyl- and methoxy- phenols evolved in the flash pyrolysis of the samples at different temperatures: a) 400 °C; b) 500 °C; c) 600 °C; d) 800 °C.

2022). This type of analysis does not allow directly comparing yields between different species, but it does allow the evolution of the yields of the same compound under different conditions. Table 8 shows the main components detected, with area percentages higher than 1% at least in one of the chromatograms and a percentage of similarity with libraries higher than 90%.

As can be seen, the main peak corresponds to CO_2 (mixed with water), with area percentages from around 10% for the bagasse (S0) up to more than 30% in the case of SNa sample. The area percentage of CO_2 is always higher in samples impregnated with alkaline catalysts. Except at 400 °C, NaOH generates a higher percentage of CO_2 than KOH does. This is coherent with the fact that NaOH leads to a higher percentage of char, showing that this catalyst favors charring + decarboxylation reactions in a major extension.

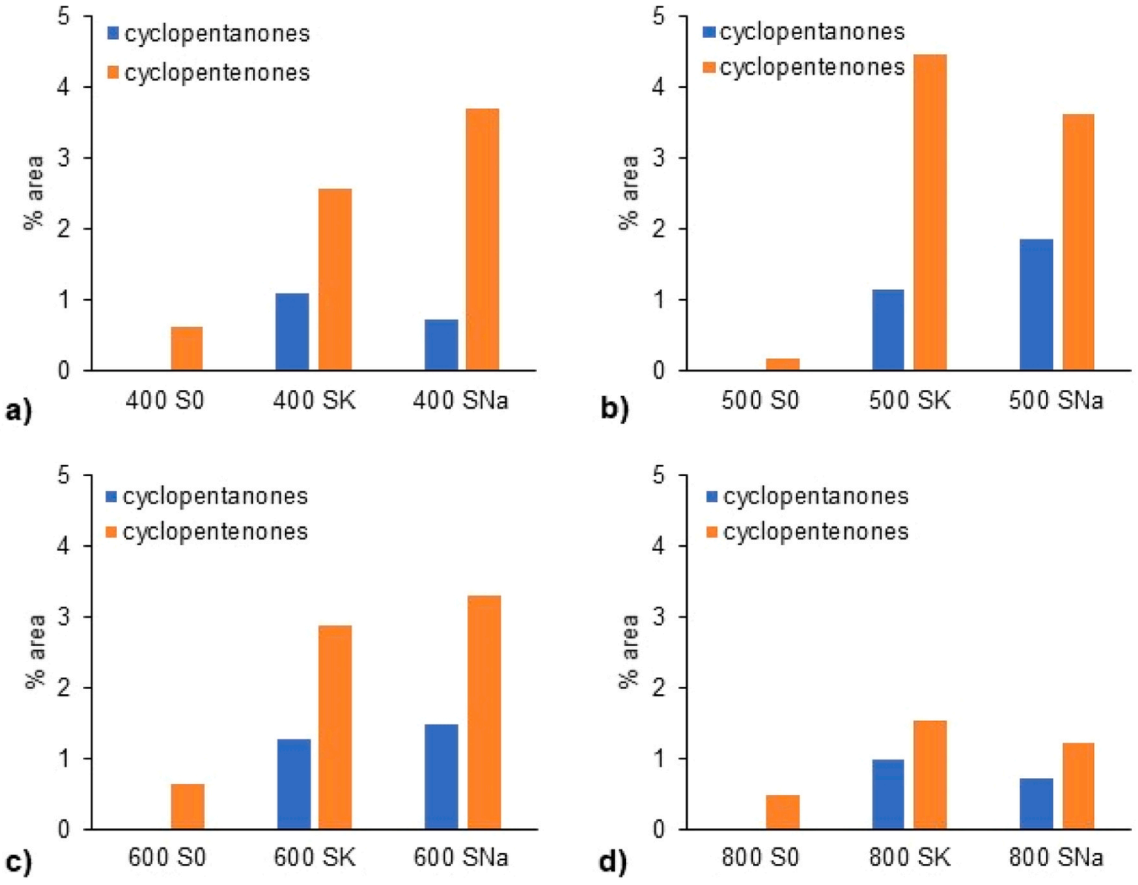

Fig. 13. Percentage of the chromatographic area corresponding to the cyclopentanone and cyclopentenone derivatives evolved in the flash pyrolysis of the samples at different temperatures: a) 400 °C; b) 500 °C; c) 600 °C; d) 800 °C.

As can be observed in Table 8, some of these major compounds are only detected in the thermal degradation of bagasse. Thus, levoglucosane, 2-hydroxycyclopent-2-en-1-one, furfural, acetic acid and hydroxyacetaldehyde cannot be detected under the presence of hydroxydes. The absence of levoglucosane under these conditions supports, once again, the idea that hydroxides are favoring charring and decarboxylation reactions over depolymerization mechanisms (Sebestyén et al., 2013). The fact that acetic acid, a primary product formed from the hemicellulose decomposition (Shafizadeh et al., 1972; Zhou et al., 2017), has not been detected in the pyrolysis of the impregnated samples, emphasizes the influence of hydroxides on the structure and/or decomposition of the hemicellulose.

On the other hand, the results show that hydroxides promote the removal of vinyl groups in the phenolic compounds. This idea agrees with that previously published about the influence of alkaline catalysts on the removal of unsaturated alkyl branch chains (Wang et al., 2022a).

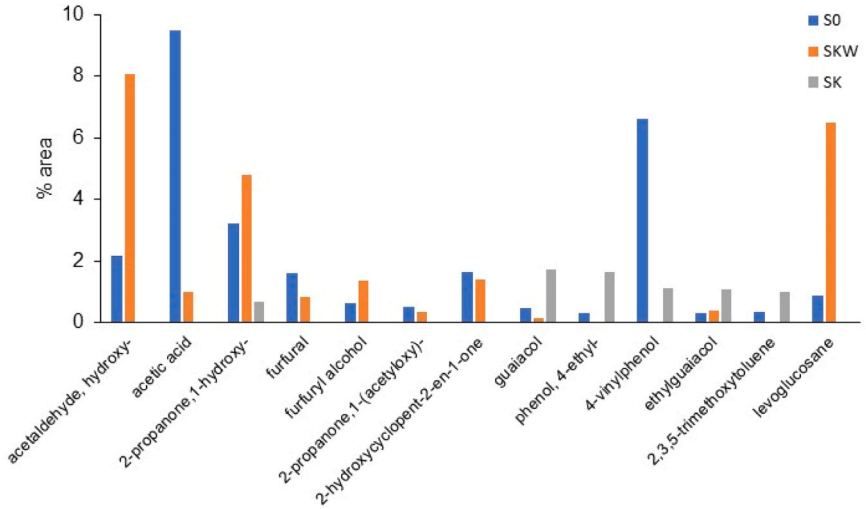

Fig. 14. Comparison among chromatographic area percentages corresponding to the main volatiles evolved in the flash pyrolysis at 400 °C of the untreated and KOH treated samples.

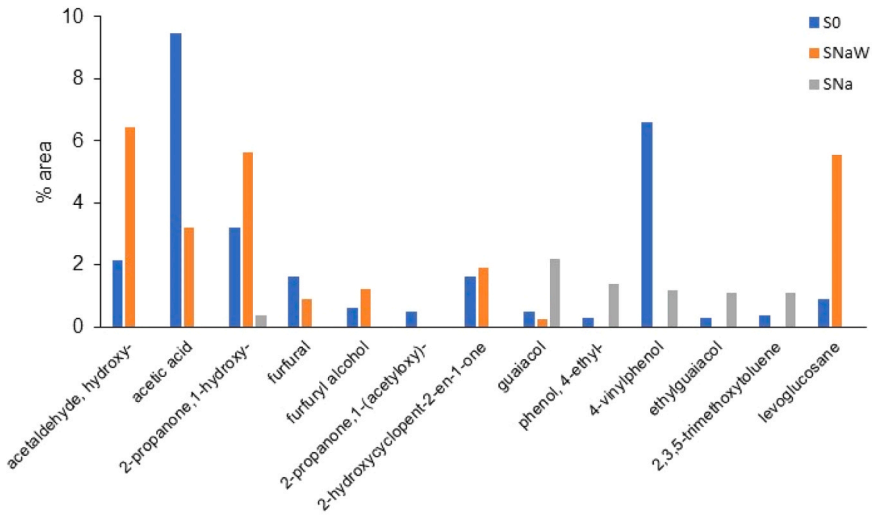

Fig. 15. Comparison among chromatographic area percentages corresponding to the main volatiles evolved in the flash pyrolysis at 400 °C of the untreated and NaOH treated samples.

Thus, among the main phenols detected, 4-vinylphenol is clearly the major one in S0 pyrolysis, with percentages 2.5–6 times higher than those in SK and SNa pyrolysis, followed by 4-vinylguaiacol. On the contrary, guaiacol is formed from alkaline samples in percentages 1.8–5 times higher than in bagasse pyrolysis. Phenol is generated in the decomposition of SK and SNa from the lowest temperature, while it is only detected in the decomposition of S0 at the highest one.

Besides the phenolic compounds shown in Table 8, flash pyrolysis of both, the original sample and those treated with alkali, generates a broad list of phenol derivatives (alkyl- and methoxy-phenols) in lower proportions. The addition of their yields leads to significant values of area percentages for these groups. Fig. 12 shows these values as a function of temperature and sample type.

According to the results shown, KOH and NaOH favor the deoxygenation reaction of the methoxy group, which agrees with other results previously reported (Wang et al., 2022a), since when temperature increases, the percentage of alkyl-phenolic compounds is clearly increased over that of the methoxy-phenols in SK and SNa samples. At the highest temperature, the methoxy group in the phenols has been removed and only alkyl-phenols have been found independently of the sample type.

In addition to the phenolic derivatives, although in a smaller proportion, the significant number of cyclopentanone and cyclopentenone derivatives obtained is noteworthy, especially remarkable in SK and SNa samples. Fig. 13 shows the area percentages of these groups, which include different derivatives and isomers of these compounds.

According to the results shown in Fig. 13, the effect of both catalysts on the distribution of these compounds is evident. Under thermal decomposition, no cyclopentanones are detected from the bagasse sample and only a low percentage of cyclopentenones is observed. This behavior is independent of the process temperature. However, the percentages of both groups increase significantly under catalytic pyrolysis in the range 400–600 °C, reducing their proportion at high temperatures. The increase of these groups of compounds under the presence of basic catalysts, attributable to ketonization reactions, has been already reported, mainly using alkaline earth metal oxide catalysts (Stefanidis et al., 2016; Hassan et al., 2020).

3.4.2. *Influence of alkali removal*

After washing SK and SNa until neutral pH, flash pyrolysis of SKW and SNaW were performed at 400 °C. As in the pyrolysis of previous samples, CO_2 + water were the major compounds obtained, with an area percentage around 15% in both cases. This value is closer to that obtained in the thermal decomposition of bagasse (around 10%) than in catalytic pyrolysis (28% SNa or 35% in SK).

Figs. 14 and 15 show the main compounds obtained in the pyrolysis of these samples (except CO_2 + water), compared to the values obtained in the pyrolysis of S0, SK and SNa at the same temperature.

Similar conclusions can be obtained from both figures. Alkaline washing has modified the sample structure, solubilizing most of the labile lignin fraction in samples and consequently, the percentage of phenols obtained in the flash pyrolysis at 400 °C is almost nil. The treatment has also reduced the acetyl groups of hemicellulose, reducing the acetic acid percentage. On the other hand, compounds such as levoglucosane, hydroxyacetaldehyde and 1-hydroxy-2-propanone, mainly coming from the cellulose decomposition, have increased their area percentages significantly (levoglucosane is increased by around 6 times and 3–4 times in the case of hydroxyacetaldehyde), thus increasing the selectivity of the process.

4. Conclusions

The valorization of sugarcane bagasse through pyrolysis allows obtaining products of interest such as biochar and volatiles with high added-value.

Under slow pyrolysis, the sugarcane bagasse produced around 18% of biochar. This amount is clearly increased by impregnating the sample with basic catalysts. By using KOH or NaOH in a ratio 1:1 (sample: catalyst), the biochar percentage is increased up to 26% and 41%, respectively. This fact could be used to obtain activated carbon through a carbonization and chemical activation process in a single step, maximizing carbon yield by optimizing operating conditions.

In addition to CO_2 and water, acetic acid and 4-vinylphenol (at 400–500 °C) and levoglucosane (at 600 °C) are the main compounds obtained in the flash pyrolysis of sugarcane bagasse. By using KOH and NaOH as pyrolytic catalysts, a significant increase in CO_2 is observed. Thus, a lower percentage of oxygen remains in the bio-oil, therefore increasing its calorific value. By comparing the volatiles obtained under basic catalytic flash pyrolysis with those from thermal flash pyrolysis, a drastic reduction of the main compounds detected under thermal conditions is produced, while an increase of phenol, guaiacol and cyclopentenone derivatives is observed. Despite the increase of guaiacol, the global percentage of methoxy-phenols is clearly decreased with alkaline catalysts.

Flash pyrolysis at 400 °C of sugarcane bagasse after alkaline hydrolysis leads to a significant reduction of acetic acid and phenol derivatives besides a significant increase of levoglucosane,

hydroxyacetaldehyde and 1-hydroxy-2-propanone. This reduction in the pyrolytic compound spectrum allows increasing the selectivity of the process.

CRediT authorship contribution statement

Rosero Marco: Writing – original draft, Investigation, Funding acquisition. **Muñoz Morayma:** Writing – original draft, Investigation, Funding acquisition. **Marcilla Antonio:** Writing – review & editing, Supervision, Funding acquisition, Formal analysis, Conceptualization. **Garcia Angela N.:** Writing – review & editing, Supervision, Funding acquisition, Formal analysis, Conceptualization.

Declaration of Competing Interest

The authors declare that they have no known competing financial interests or personal relationships that could have appeared to influence the work reported in this paper.

Data Availability

Data will be made available on request.

Acknowledgements

This research was funded by 'Conselleria d'Educació, Investigació, Cultura i Esport' (IDIFEDER 2018/009) and 'Universidad Central del Ecuador' (International Collaboration Agreement No 061-P-05).

References

Amenaghawon, A.N., Anyalewechi, C.L., Okieimen, C.O., Kusuma, H.S., 2021. Biomass pyrolysis technologies for value-added products: a state-of-the-art review. Environ. Dev. Sustain. 23, 14324–14378. https://doi.org/10.1007/s10668-021-01276-5.

Antal Jr, M.J., Mok, W.S.L., Varhegyi, G., Szekely, T., 1990. Review of methods for improving the yield of charcoal from biomass. Energy Fuels 4, 221–225.

Antunes, F., Mota, I.F., Da Silva Burgal, J., Pintado, M., 2022. A review on the valorization of lignin from sugarcane by-products: from extraction to application. Biomass Bioenergy 166, 106603. https://doi.org/10.1016/j.biombioe.2022.106603.

Aruna, Bagotia, N., Sharma, A.K., Kumar, S., 2021. A review on modified sugarcane bagasse biosorbent for removal of dyes. Chemosphere 268, 129309. https://doi.org/10.1016/j.chemosphere.2020.129309.

Balahmar, N., Al-Jumialya, A.S., Mokaya, R., 2017. Biomass to porous carbon in one step: directly activated biomass for high performance CO_2 storage. J. Mater. Chem. A 5, 12330–12339. https://doi.org/10.1039/c7ta01722g.

Bañón, E., Marcilla, A., García, A.N., Martínez, P., León, M., 2016. Kinetic model of the thermal pyrolysis of chrome tanned leather treated with NaOH under different conditions using thermogravimetric analysis. Waste Manag. 48, 285–299. https://doi.org/10.1016/j.wasman.2015.10.012.

Bartos, A., Anggono, J., Farkas, Á.E., Kun, D., Soetaredjo, F.E., Móczó, J., Antoni, Purwaningsih, H., Pukánszky, B., 2020. Alkali treatment of lignocellulosic fibers extracted from sugarcane bagasse: Composition, structure, properties. Polym. Test. 88, 106549 https://doi.org/10.1016/j.polymertesting.2020.106549.

Channiwala, S.A., Parikh, P.P., 2002. A unified correlation for estimating HHV of solid, liquid and gaseous fuels. Fuel 81, 1051–1063.

Chen, D., Wang, Y., Liu, Y., Cen, K., Cao, X., Ma, Z., Li, Y., 2019. Comparative study on the pyrolysis behaviors of rice straw under different washing pretreatments of water, acid solution, and aqueous phase bio-oil by using TG-FTIR and Py-GC/MS. Fuel 252, 1–9. https://doi.org/10.1016/j.fuel.2019.04.086.

CINCAE, 2013. Utilización de subproductos de la caña de azúcar y de la industria alcoholera ecuatoriana para uso en la fertilización en los cultivos de caña. Centro de investigación de la caña de azúcar del Ecuador. ⟨https://cincae.org⟩ (Revised on 3 July 2023).

Costa, A.G., Pinheiro, G.C., Pinheiro, F.G.C., Dos Santos, A.B., Santaella, S.T., Leitão, R. C., 2014. The use of thermochemical pretreatments to improve the anaerobic biodegradability and biochemical methane potential of the sugarcane bagasse. Chem. Eng. J. 248, 363–372. https://doi.org/10.1016/j.cej.2014.03.060.

DeGroot, W.F., Shafizadeh, F., 1984. The influence of exchangeable cations on the carbonization of biomass. J. Anal. Appl. Pyrol 6, 217–232. https://doi.org/10.1016/0165-2370(84)80019-4.

Deng, W., Feng, Y., Fu, J., Guo, H., Guo, Y., Han, B., Jiang, Z., Kong, L., Li, C., Liu, H., Nguyen, P.T.T., Ren, P., Wang, F., Wang, S., Wang, Y., Wang, Y., Wong, S.S., Yan, K., Yan, N., Yang, X., Zhang, Y., Zhang, Z., Zeng, X., Zhou, H., 2023. Catalytic conversion of ignocellulosic biomass into chemicals and fuels. Green. Energy Environ. 8, 10–114. https://doi.org/10.1016/j.gee.2022.07.003.

Díaz, R., 2008. Caracterización Energética del Bagazo de Caña de Azúcar del Ingenio Valdez. Ecuador. Curso Internacional 'Producción y Aprovechamiento energético de biomasa', 8-12 Septiembre.

Esperanza, M.M., García, A.N., Font, R., Conesa, J.A., 1999. Pyrolysis of varnish wastes based on a polyurethane. J. Anal. Appl. Pyrolysis 52, 151–166.

Fisher, T., Hajaligol, M., Waymack, B., Kellogg, D., 2002. Pyrolysis behavior and kinetics of biomass derived materials. J. Anal. Appl. Pyrol 62, 331–349. https://doi.org/10.1016/S0165-2370(01)00129-2.

Fu, X., Wang, X., Li, Y., Xin, Y., Li, S., 2019. Enhancing and upgrading bio-oil during catalytic pyrolysis of cellulose: the synergistic effect of potassium cation and different anions impregnation. Fuel Process Technol. 193, 338–347. https://doi.org/10.1016/j.fuproc.2019.05.022.

García, A.N., Font, R., 2004. Thermogravimetric kinetic model of the pyrolysis and combustion of an ethylene-vinyl acetate copolymer refuse. Fuel 83, 1165–1173. https://doi.org/10.1016/j.fuel.2003.10.029.

García, R., Pizarro, C., Lavín, A.G., Bueno, J.L., 2013. Biomass proximate analysis using thermogravimetry. Bioresour. Technol. 139, 1–4. https://doi.org/10.1016/j.biortech.2013.03.197.

García-Pérez, M., Chaala, A., Yang, J., Roy, C., 2001. Co-pyrolysis of sugarcane bagasse with petroleum residue. Part I: thermogravimetric analysis. Fuel 80, 1245–1258.

Gómez-Siurana, A., Marcilla, A., Beltrán, M., Berenguer, D., Martínez-Castellanos, I., Menargues, S., 2013. TGA/FTIR study of tobacco and glycerol–tobacco mixtures. Thermochim. Acta 573, 146–157. https://doi.org/10.1016/j.tca.2013.09.007.

Haghdan, S., Renneckar, S., Smith, G.D., 2016. 1 - Sources of Lignin in Lignin in Polymer Composites. William Andrew Publishing, pp. 1–11. https://doi.org/10.1016/B978-0-323-35565-0.00001-1.

Hassan, N.S., Jalil, A.A., Hitam, C.N.C., Vo, D.V.N., Nabgan, W., 2020. Biofuels and renewable chemicals production by catalytic pyrolysis of cellulose: a review. Environ. Chem. Lett. 18, 1625–1648. https://doi.org/10.1007/s10311-020-01040-7.

Hirunpraditkoon, S., García, A.N., 2009. Kinetic study of vetiver grass powder filled polypropylene composites. Thermochim. Acta 482, 30–38. https://doi.org/10.1016/j.tca.2008.10.004.

Kanwal, S., Chaudhry, N., Munir, S., Sana, H., 2019. Effect of torrefaction conditions on the physicochemical characterization of agricultural waste (sugarcane bagasse). Waste Manag. 88, 280–290. https://doi.org/10.1016/j.wasman.2019.03.053.

Karatepe, N., Küçükbayrak, S., 1993. Proximate analysis of some Turkish lignites by thermogravimetry. Thermochim. Acta 213, 147–150. https://doi.org/10.1016/0040-6031(93)80012-Y.

Londoño-Larrea, P., Villamarin-Barriga, E., García, A.N., Marcilla, A., 2022. Study of cocoa pod husks thermal decomposition. Appl. Sci. 12, 9318. https://doi.org/10.3390/app12189318.

Mahmud, M.A., Anannya, F.R., 2021. Sugarcane bagasse - a source of cellulosic fiber for diverse applications. Heliyon 7, e07771. https://doi.org/10.1016/j.heliyon.2021.e07771.

Mankar, A.R., Pandey, A., Modak, A., Pant, K.K., 2021. Pretreatment of lignocellulosic biomass: a review on recent advances. Bioresour. Technol. 334, 125235 https://doi.org/10.1016/j.biortech.2021.125235.

Marathe, P.S., Oudenhoven, S.R.G., Heerspink, P.W., Kersten, S.R.A., Westerhof, R.J.M., 2017. Fast pyrolysis of cellulose in vacuum: the effect of potassium salts in the primary reactions. Chem. Eng. J. 329, 187–197. https://doi.org/10.1016/j.jaap.2022.105479.

Marcilla, A., Gómez-Siurana, A., Gomis, C., Chápuli, E., Catalá, M.C., Valdés, F.J., 2009. Characterization of microalgal species through TGA/FTIR analysis: application to nannochloropsis sp. Thermochim. Acta 484, 41–47. https://doi.org/10.1016/j.tca.2008.12.005.

Martinez-Escandell, M., Monteiro de Castro, M., Molina-Sabio, M., Rodriguez-Reinoso, F., 2013. KOH activation of carbon materials obtained from the pyrolysis of ethylene tar at different temperatures. Fuel Process. Technol. 106, 402–407. https://doi.org/10.1016/j.fuproc.2012.09.005.

Motaung, T.E., Anandjiwala, R.D., 2015. Effect of alkali and acid treatment on thermal degradation kinetics of sugar cane bagasse. Ind. Crop Prod. 74, 472–477. https://doi.org/10.1016/j.indcrop.2015.05.062.

Mothé, C.G., de Miranda, I.C., 2013. Study of kinetic parameters of thermal decomposition of bagasse and sugarcane straw using Friedman and Ozawa–Flynn–Wall isoconversional methods. J. Therm. Anal. Calor. 113, 497–505. https://doi.org/10.1007/s10973-013-3163-7.

Munir, S., Daood, S.S., Nimmo, W., Cunliffe, A.M., Gibbs, B.M., 2009. Thermal analysis and devolatilization kinetics of cotton stalk, sugar cane bagasse and shea meal under nitrogen and air atmospheres. Bioresour. Technol. 100, 1413–1418. https://doi.org/10.1016/j.biortech.2008.07.065.

Naron, D.R., Collard, F.-X., Tyhoda, L., Görgens, J.F., 2019. Influence of impregnated catalyst on the phenols production from pyrolysis of hardwood, softwood, and herbaceous lignins. Ind. Crop Prod. 131, 348–356. https://doi.org/10.1016/j.indcrop.2019.02.001.

Nunes, L.J.R., Loureiro, L.M.E.F., Sá, L.C.R., Silva, H.F.C., 2020. Sugarcane industry waste recovery: a case study using thermochemical conversion technologies to increase sustainability. Appl. Sci. 10, 6481. https://doi.org/10.3390/app10186481.

Ounas, A., Aboulkas, A., El Harfi, K., Bacaoui, A., Yaacoubi, A., 2011. Pyrolysis of olive residue and sugar cane bagasse: non-isothermal thermogravimetric kinetic analysis. Bioresour. Technol. 102, 11234–11238. https://doi.org/10.1016/j.biortech.2011.09.010.

Peng, Y., Wu, S., 2011. Fast pyrolysis characteristics of sugarcane bagasse hemicellulose. Cellul. Chem. Technol. 45 (9-10), 605–612.

Rocha, G.Jd.M., Nascimento, V.M., Gonçalves, A.R., Silva, V.F.N., Martín, C., 2015. Influence of mixed sugarcane bagasse simples evaluated by elemental and physical-

chemical composition. Ind. Crop Prod. 64, 52–58. https://doi.org/10.1016/j.indcrop.2014.11.003.
Rueda-Ordóñez, Y.J., Tannous, K., 2017. Análisis cinético de la descomposición térmica de biomasas aplicando un esquema de reacciones paralelas independientes. UIS Ing. í 16, 119–128. https://doi.org/10.18273/revuin.v16n2-2017011.
Ruiz Beviá, F., Prats Rico, D., Marcilla Gomis, A.F., 1984. Activated carbon from almond shells. Chemical activation. 1. Activating reagent selection and variables influence. Ind. Eng. Chem. Prod. Res Dev. 23, 266–269.
Schmitt, C.C., Moreira, R., Neves, R.C., Richter, D., Funke, A., Raffelt, K., Grunwaldt, J.-D., Dahmen, N., 2020. From agriculture residue to upgraded product: the thermochemical conversion of sugarcane bagasse for fuel and chemical products. Fuel Process Technol. 197, 106199 https://doi.org/10.1016/j.fuproc.2019.106199.
Sebestyén, Z., May, Z., Réczey, K., Jakab, E., 2011. The effect of alkaline pretreatment on the thermal decomposition of hemp. J. Therm. Anal. Calor. 105, 1061–1069. https://doi.org/10.1007/s10973-010-1056-6.
Sebestyén, Z., Jakab, E., May, Z., Sipos, B., Réczey, K., 2013. Thermal behavior of native, washed and steam exploded lignocellulosic biomass samples. J. Anal. Appl. Pyrol 101, 61–71. https://doi.org/10.1016/j.jaap.2013.02.011.
Shafizadeh, F., McGinnis, G.D., Philpot, C.W., 1972. Thermal degradation of xylan and related model compounds. Carbohydr. Res. 25, 23–33. https://doi.org/10.1016/S0008-6215(00)82742-1.
Shen, Y., Zhang, N., Zhang, S., 2020. Catalytic pyrolysis of biomass with potassium compounds for Co-production of high-quality biofuels and porous carbons. Energy 190, 116431. https://doi.org/10.1016/j.energy.2019.116431.
Soomro, M., Tam, V.W.Y., Jorge Evangelista, A.C., 2023. 3 - Industrial and agro-waste materials for use in recycled concrete in Recycled Concrete. Woodhead Publishing Series in Civil and Structural Engineering, 47-117. https://doi.org/10.1016/B978-0-323-85210-4.00009-6.
Stefanidis, S.D., Karakoulia, S.A., Kalogiannis, K.G., Iliopoulou, E.F., Delimitis, A., Yiannoulakis, H., Zampetakis, T., Lappas, A.A., Triantafyllidis, K.S., 2016. Natural magnesium oxide (MgO) catalysts: a cost-effective sustainable alternative to acid zeolites for the in situ upgrading of biomass fast pyrolysis oil. Appl. Catal. B-Environ. 196, 155–173. https://doi.org/10.1016/j.apcatb.2016.05.031.
The Science Agriculture. Agriculture and Science with trusted data. ⟨https://scienceagri.com/10-worlds-biggest-sugarcane-producers/⟩ (Revised on 18 July 2023).
Tsai, W.T., Lee, M.K., Chang, Y.M., 2006. Fast pyrolysis of rice straw, sugarcane bagasse and coconut shell in an induction-heating reactor. J. Anal. Appl. Pyrol 76, 230–237. https://doi.org/10.1016/j.jaap.2005.11.007.
Vyazovkin, S., Burnham, A.K., Criado, J.M., Pérez-Maqueda, L.A., Popescu, C., Sbirrazzuoli, N., 2011. ICTAC Kinetics Committee recommendations for performing kinetic computations on thermal analysis data. Thermochim. Acta 520, 1–19. https://doi.org/10.1016/j.tca.2011.03.034.
Wang, W., Lemaire, R., Bensakhria, A., Luart, D., 2022a. Review on the catalytic effects of alkali and alkaline earth metals (AAEMs) including sodium, potassium, calcium and magnesium on the pyrolysis of lignocellulosic biomass and on the co-pyrolysis of coal with biomass. J. Anal. Appl. Pyrol 163, 105479. https://doi.org/10.1016/j.cej.2017.05.134.
Wang, D., Tian, J., Guan, J., Ding, Y., Wang, M.L., Tonnis, B., Liu, J., Huang, Q., 2022b. Valorization of sugarcane bagasse for sugar extraction and residue as an adsorbent for pollutant removal. Front Bioeng. Biotech. 10 https://doi.org/10.3389/fbioe.2022.893941.
Williams, N.E., Oba, O.A., Aydinlik, N.P., 2022. Modification, production, and methods of KOH-activated carbon. ChemBioEng Rev. 9, 164–189. https://doi.org/10.1002/cben.202100030.
Yang, H., Yan, R., Chen, H., Lee, D.H., Zheng, C., 2007. Characteristics of hemicellulose, cellulose and lignin pyrolysis. Fuel 86, 1781–1788. https://doi.org/10.1016/j.fuel.2006.12.013.
Yu, J., Paterson, N., Blamey, J., Millan, M., 2017. Cellulose, xylan and lignin interactions during pyrolysis of lignocellulosic biomass. Fuel 191, 140–149. https://doi.org/10.1016/j.fuel.2016.11.057.
Zhou, L., Jia, Y., Nguyen, T.H., Adesina, A.A., Liu, Z., 2013. Hydropyrolysis characteristics of potassium-impregnated pine wood. Fuel Process Technol. 116, 149–157. https://doi.org/10.1016/j.fuproc.2013.05.005.
Zhou, X., Li, W., Mabon, R., Broadbelt, L.J., 2017. A critical review on hemicellulose pyrolysis. Energy Technol. 5, 52–79. https://doi.org/10.1002/ente.201600327.
Zhuang, J., Li, M., Pu, Y., Ragauskas, A.J., Yoo, C.G., 2020. Observation of Potential contaminants in processed biomass using fourier transform infrared spectroscopy. Appl. Sci. 10, 4345. https://doi.org/10.3390/app10124345.